Ab Initio Study of the Atmospheric Oxidation of CS₂

Michael L. McKee*,[†] and P. H. Wine[‡]

Contribution from the Department of Chemistry, Auburn University, Auburn, Alabama 36849, and School of Chemistry and Biochemistry and School of Earth and Atmospheric Sciences, Georgia Institute of Technology, Atlanta, Georgia 30332

Abstract: The reactions of OH with CS_2, OCS, and ^{3}SO and of $^3O_2$ with CS_2, SCSOH, and HOSO have been studied by optimizing minima and transition states with B3LYP/6-31+G(d) and carrying out higher-level ab initio calculations on fixed geometries. The combined calculations provide valuable insight into the mechanism for the atmospheric oxidation of CS_2. The initial step is the formation of the SCSOH complex (**1**) which readily adds molecular oxygen to form the SC(OO)SOH complex (**8**). A key step is the oxygen atom transfer to the sulfur bearing the hydroxyl group which leads directly to OCS plus HOSO. The HOSO + $^3O_2$ reaction has a near zero calculated activation barrier so generation of O_2H + SO_2 should proceed readily in the atmosphere.

Introduction

The oxidation of carbon disulfide produces an estimated 30% of the atmospheric OCS.[1] Understanding the mechanism for transforming sulfur compounds into OCS is important because OCS is the most abundant sulfur compound in the atmosphere. Due to its kinetic and thermodynamic stability, OCS is the only sulfur compound that diffuses into the stratosphere,[1] where its photooxidation is thought to be an important contributor to the lower stratospheric aerosol layer.[2] Early direct studies of the reaction OH + CS_2 appeared to indicate that the reaction was too slow to be of relevance to atmospheric CS_2 degradation. However, in 1982 Jones et al.[3] demonstrated that the reaction was significantly faster in the presence of molecular oxygen (eqs 1 and 2). Since then, significant progress in understanding the reaction has been made.[4−15] Reaction 2 is extremely

complex, with over 25 exothermic product channels![14] The reactions of OH with SR_2[16−20] and SO_2[21−23] are other related examples of atmospheric sulfur oxidation reactions currently attracting attention.

$$OH + CS_2 + M \rightleftarrows CS_2OH + M \qquad (1)$$

$$CS_2OH + O_2 \rightarrow products \qquad (2)$$

Carbon- and sulfur-containing products of the $CS_2/OH/^3O_2$ reaction that have been directly observed include OCS, SO_2, and CO. These products are formed with yields of 0.83 ± 0.08, 1.15 ± 0.10, and 0.16 ± 0.03 per molecule of CS_2 consumed (OCS:SO_2:CO).[14] The above yields of OCS and CO are also obtained on a per molecule of OH consumed basis, and these products are formed "promptly" following flash photolytic production of OH in the presence of CS_2 and $^3O_2$;[14] in this context, a "prompt" product is defined to be one that is formed as a primary product of the $CS_2OH + ^3O_2$ reaction or via a rapid reaction of a primary product with O_2. Unlike OCS and CO, only about 75% of SO_2 is formed promptly.[14] Indirect evidence suggests that nonprompt formation of SO_2 occurs via a prompt SO intermediate.[14] In addition, O_2H has been observed as a major prompt product.[9]

[†] Auburn University.

[‡] Georgia Institute of Technology.

(1) (a) Chin, M.; Davis, D. D. *Global Biogeochem. Cycles* **1993**, *7*, 321. (b) Berresheim, H.; Wine, P. H.; Davis, D. D. Sulfur in the Atmosphere. In *Composition, Chemistry, and Climate of the Atmosphere*; Singh, H. B., Ed.; Van Nostrand Reinhold: New York, 1995; Chapter 8.

(2) Crutzen, P. J. *Geophys. Res. Lett.* **1976**, *3*, 73.

(3) (a) Jones, B. M. R.; Burrows, J. P.; Cox, R. A.; Penkett, S. A. *Chem. Phys. Lett.* **1982**, *88*, 372. (b) Jones, B. M. R.; Cox, R. A.; Penkett, S. A. *J. Atmos. Chem.* **1983**, *1*, 65.

(4) Bulatov, V. P.; Ceskis, S.; Iogansen, A. A.; Kulakov, P. V.; Sarkisov, O. M.; Hassinen, E. *Chem. Phys. Lett.* **1988**, *153*, 258.

(5) Hynes, A. J.; Wine, P. H.; Nicovich, J. M. *J. Phys. Chem.* **1988**, *92*, 3846.

(6) Lovejoy, E. R.; Kroeger, K. S.; Ravishankara, A. R. *Chem. Phys. Lett.* **1990**, *167*, 183.

(7) Murrells, T. P.; Lovejoy, E. R.; Ravishankara, A. R. *J. Phys. Chem.* **1990**, *94*, 2381.

(8) Becker, K. H.; Nelsen, W.; Su, Y.; Wirtz, K. *Chem. Phys. Lett.* **1990**, *168*, 559.

(9) Lovejoy, E. R.; Murrells, T. P.; Ravishankara, A. R.; Howard, C. J. *J. Phys. Chem.* **1990**, *94*, 2386.

(10) Diau, E. W. G.; Lee, Y. P. *J. Phys. Chem.* **1991**, *95*, 7726.

(11) Diau, E. W. G.; Lee, Y. P. *J. Phys. Chem.* **1991**, *95*, 379.

(12) Tyndall, G. S.; Ravishankara, A. R. *Int. J. Chem. Kinet.* **1991**, *23*, 483.

(13) Lovejoy, E. R.; Ravishankara, A. R.; Howard, C. J. *Int. J. Chem. Kinet.* **1994**, *26*, 551.

(14) Stickel, R. E.; Chin, M.; Daykin, E. P.; Hynes, A. J.; Wine, P. H.; Wallington, T. J. *J. Phys. Chem.* **1993**, *97*, 13653.

(15) Silvente, E.; Richter, R. C.; Hynes, A. J. *J. Chem. Soc., Faraday Trans.* **1997**, *93*, 2821.

(16) Urbanski, S. P.; Stickel, R. E.; Wine, P. H. *J. Chem. Phys. A* **1998**, *102*, 10522.

(17) Butkovskaya, N. I.; Setser, D. W. *J. Phys. Chem. A* **1998**, *102*, 6395.

(18) Butkovskaya, N. I.; Setser, D. W. *J. Phys. Chem. A* **1999**, *103*, 6921.

(19) (a) Barnes, I.; Becker, K. H.; Patroescu, I. *Geophys. Res. Lett.* **1994**, *21*, 2389. (b) Barnes, I.; Becker, K. H.; Patroescu, I. *Atmos. Environ.* **1996**, *30*, 1805. (c) Becker, K. H.; Patroescu, J. *Phys. Chem.* **1996**, *35*, 1. (d) Patroescu, I. V.; Barnes, I.; Becker, K. H.; Mihalopoulos, N. *Atmos. Environ.* **1999**, *33*, 25. Erratum: **1999**, *33*, 3083. (e) Arsene, C.; Barnes, I.; Becker, K. H. *Phys. Chem. Chem. Phys.* **1999**, *1*, 5463.
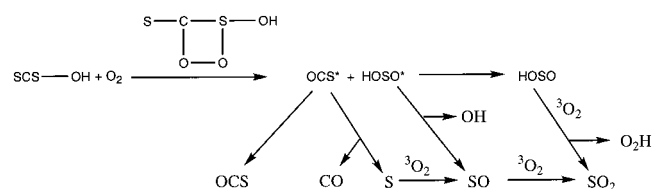
(20) Gawandi, V. B.; Mohan, H.; Mittal, J. P. *J. Chem. Soc., Perkin Trans. 2* **1999**, 1425.

(21) Fulle, D.; Hamann, H. F.; Hippler, H. *Phys. Chem. Chem. Phys.* **1999**, *1*, 2695.

(22) Majumdar, D.; Kim, G.-S.; Kim, J.; Oh, K. S.; Lee, J. Y.; Kim, K. S.; Choi, W. Y.; Lee, S.-H.; Kang, M.-H.; Mhin, B. J. *J. Chem. Phys.* **2000**, *112*, 723.

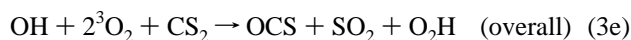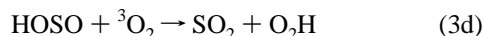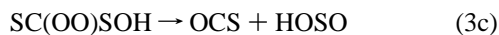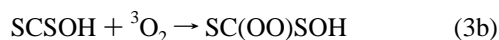(23) Li, W.-K.; McKee, M. L. *J. Phys. Chem. A* **1997**, *101*, 9745.

Scheme 1

A mechanism for the reaction of O_2 with the proposed adduct[13,14] that is consistent with the above experimental observations is shown in Scheme 1. However, no computational support for the mechanism has been presented.

Using the laser flash photolysis laser induced fluorescence (LFP-LIF) technique, Wahner and Ravishankara[24] studied the reaction of OH and OCS in the presence of O_2. In contrast to the CS_2/OH/O_2 reaction system, the reaction did not show an oxygen enhancement in the rate. The authors concluded that the OCS−OH adduct was not stable enough to have a significant lifetime.

Calculations will be presented below for reactions given in eqs 3a−e which are relevant to the mechanism of atmospheric oxidation of CS_2.

$$OH + CS_2 \rightarrow SCSOH \qquad (3a)$$

$$SCSOH + {}^3O_2 \rightarrow SC(OO)SOH \qquad (3b)$$

$$SC(OO)SOH \rightarrow OCS + HOSO \qquad (3c)$$

$$HOSO + {}^3O_2 \rightarrow SO_2 + O_2H \qquad (3d)$$

$$OH + 2{}^3O_2 + CS_2 \rightarrow OCS + SO_2 + O_2H \quad \text{(overall)} \quad (3e)$$

Computational Methods

The density functional theory exchange/correlation combination of B3/LYP has been used with the 6-31+G(d) basis set for geometry optimization. This level of theory has proven to be effective in reproducing geometries in a wide variety of bonding environments.[25,26] Vibrational frequencies have been computed at the B3LYP/6-31+G-(d) level to confirm the nature of the stationary points and to make zero-point corrections. The imaginary frequency (transition vector) was animated graphically for all transition states to ensure that the motion was appropriate for converting reactants to products. Such a test is evidence but not proof that a relationship exists between reactant, transition state, and product. Single-point calculations have been made at QCISD(T)/6-31G(d) and MP2/6-311+G(3df,2p) levels and combined with the additivity approximation[27] to estimate relative energies at the [QCISD(T)/6-311+G(3df,2p)] level (eq 4).

$$\Delta E(\text{QCISD(T)/6-311+G(3df,2p)}) \approx \Delta E(\text{QCISD(T)/6-31G(d)}) + \\ \Delta E(\text{MP2/6-311+G(3df,2p)}) - \Delta E(\text{MP2/6-31G(d)}) \quad (4)$$

The approximation in eq 4 is similar to the one used in the G2-(MP2,SVP) procedure[28] except that geometries and zero-point energies (unscaled) are calculated at B3LYP/6-31+G(d) rather than MP2/6-31G-

(d) (for geometry) and HF/6-31G(d) (for frequencies) and a higher-level-correction term (ΔHLC) has not been included. The ΔHLC term is zero except when the number of α and β spin electrons is different from the reference compound. For example, forming the adduct SC-(OO)SOH (**8A/8B/8C**) from CS_2 + OH + ${}^3O_2$ would involve a higher-level-correction (ΔHLC) of 3.1 kcal/mol because the number of α and β electrons differ. With the exception of the reactant ${}^3O_2$ and product ${}^3SO$, all reactions occur on the doublet surface where the ΔHLC term is zero. Thus, the target calculation [QCISD(T)/6-311+G(3df,2p)] is similar to the G2(MP2,SVP) method which has been shown by Radom and co-workers[28a] to reproduce a number of molecular properties to within chemical accuracy (2 kcal/mol). However, it should be pointed out that for transition states and systems with significant spin contamination the errors may be larger.

Tables of total energies (hartrees) and zero-point energies (kcal/mol) as well as Cartesian coordinates of all species are provided as Supporting Information. The discussion will focus on six different sections of the potential energy surface: Section A (OH + CS_2); Section B (OH + OCS); Section C (SCSOH + ${}^3O_2$); Section D (${}^3SO$ + OH); Section E (HOSO + ${}^3O_2$); Section F (CS_2 + ${}^3O_2$). A table of relative energies, enthalpies, and free energies is presented (Table 1) for species on the potential energy surfaces for Sections A−F. In the discussion below, standard energy values will be enthalpies at 298 K computed from eq 7 with zero-point and heat capacity corrections made from B3LYP/6-31+G(d) frequencies. All calculations (including CASSCF calculations discussed later) were made with the GAUSSIAN98 program.[29] The frozen core approximation was used in calculating MP2 and QCISD(T) energies. Corrections for basis set superposition errors (BSSE) have not been made.

Results and Discussion

Section A (OH + CS_2). The addition of the OH radical to sulfur to form an S-adduct has been of great interest to atmospheric chemists.[1−23] In the case of dimethyl sulfide (SMe_2), the complex is bound to sulfur via a 2c−3e bond with a bond energy of about 10 kcal/mol.[30] Early calculations of the OH radical with CS_2 indicated that OH could attach to the carbon atom to form a stable complex (C-adduct), while the S-adduct was computed to be endothermic.[31] Later calculations at a higher level of theory found that both adducts were stable; the S-adduct was bound by 5.9 kcal/mol while the C-adduct was bound by 30.3 kcal/mol.[32] The S-adduct was predicted to form without activation while formation of the C-adduct had an activation barrier of 7.0 kcal/mol.[32] The existence of an S-adduct is consistent with LFP-LIF experiments by Hynes et al.[5] and Murrells et al.,[7] who observed a negative enthalpic barrier for formation of the adduct with a total binding enthalpy of between 9.9 and 10.9 kcal/mol.

In the present study, the C- and S-adducts have been reinvestigated at higher levels of theory. In Table 2, geometric

(24) Wahner, A.; Ravishankara, A. R. *J. Geophys. Chem.* **1987**, *92*, 2189.

(25) Bartolotti, L. J.; Flurchick, K. An Introduction to Density Functional Theory. In *Reviews in Computational Chemistry*; Lipkowitz, K. B., Boyd, D. B., Eds.; VCH: New York, 1996; Vol. 7.

(26) Koch, W.; Holthausen, M. C. *A Chemist's Guide to Density Functional Theory*; Wiley-VCH: New York, 2000.

(27) (a) McKee, M. L.; Lipscomb, W. N. *J. Am. Chem. Soc.* **1981**, *103*, 4673. (b) Nobes, R. H.; Bouma, W. J.; Radom, L. *Chem. Phys. Lett.* **1982**, *89*, 497. (c) McKee, M. L.; Lipscomb, W. N. *Inorg. Chem.* **1985**, *24*, 762.

(28) (a) Smith, B. J.; Radom, L. *J. Phys. Chem.* **1995**, *99*, 6468. (b) Curtiss, L. A.; Redfern, P. C.; Smith, B. J.; Radom, L. *J. Chem. Phys.* **1996**, *104*, 5148. (c) Nicolaides, A.; Rauk. A.; Glukhovtsev, M. N.; Radom, L. *J. Phys. Chem.* **1996**, *100*, 17460.

(29) Frisch, M. J.; Trucks, G. W.; Schlegel, H. B.; Scuseria, G. E.; Robb, M. A.; Cheeseman, J. R.; Zakrzewski, V. G.; Montgomery, J. A., Jr.; Stratmann, R. E.; Burant, J. C.; Dapprich, S.; Millam, J. M.; Daniels, A. D.; Kudin, K. N.; Strain, M. C.; Farkas, O.; Tomasi, J.; Barone, V.; Cossi, M.; Cammi, R.; Mennucci, B.; Pomelli, C.; Adamo, C.; Clifford, S.; Ochterski, J.; Petersson, G. A.; Ayala, P. Y.; Cui, Q.; Morokuma, K.; Malick, D. K.; Rabuck, A. D.; Raghavachari, K.; Foresman, J. B.; Cioslowski, J.; Ortiz, J. V.; Stefanov, B. B.; Liu, G.; Liashenko, A.; Piskorz, P.; Komaromi, I.; Gomperts, R.; Martin, R. L.; Fox, D. J.; Keith, T.; Al-Laham, M. A.; Peng, C. Y.; Nanayakkara, A.; Gonzalez, C.; Challacombe, M.; Gill, P. M. W.; Johnson, B. G.; Chen, W.; Wong, M. W.; Andres, J. L.; Head-Gordon, M.; Replogle, E. S.; Pople, J. A. *Gaussian 98*; Gaussian, Inc.: Pittsburgh, PA, 1998.

(30) (a) Hynes, A. J.; Stoker, R. B.; Pounds, A. J.; McKay, T.; Bradshaw, J. D.; Nicovich, J. M.; Wine, P. H. *J. Phys. Chem.* **1995**, *99*, 16967. (b) Barone, S. B.; Turnipseed, A. A.; Ravishankara, A. R. *J. Phys. Chem.* **1996**, *100*, 14694.

(31) Lunell, S.; Huang, M. B.; Sahetchian, K. A.; Chachaty, C.; Zabel, F. *J. Chem. Soc., Chem. Commun.* **1990**, *14*, 949.

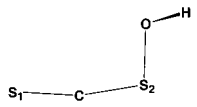(32) McKee, M. L. *Chem. Phys. Lett.* **1993**, *201*, 41.

Table 1. Relative Energies (hartrees) at Various Levels of Theory for Species Optimized at B3LYP/6-31+G(d)[a]

	B3LYP/II	+ZPC	MP2/I	QCISD(T)/I	MP2/III	[QCISD(T)/II I]	+ZPC	ΔH(298K)	ΔG(298K)
Section A (OH + SCS)	0.0	0.0	0.0	0.0	0.0	0.0	0.0	0.0	0.0
SCSOH (**1**)	−6.4	−4.1	2.3	0.4	−6.1	−8.0	−5.7	−6.4	0.6
TS1/2	5.0	6.7	15.7	10.1	14.6	9.0	10.7	9.5	17.5
SC(OH)S (**2**)	−35.4	−31.2	−26.6	−30.2	−30.8	−34.4	−30.2	−31.6	−23.2
TS2/3	−0.4	−0.2	4.8	5.4	0.8	1.4	1.6	0.1	8.7
SC(O)SH (**3**)	−31.1	−29.3	−27.0	−27.8	−27.9	−28.7	−26.9	−27.9	−20.2
TS3/(OCS + SH)	−28.0	−27.1	−21.6	−21.6	−25.0	−25.0	−24.1	−25.2	−17.4
OCS + SH	−36.4	−36.4	−38.5	−36.1	−37.5	−35.1	−35.1	−34.9	−35.5
TS1/(CS + SOH)	33.5	34.7	37.1	32.9	36.5	32.3	33.5	33.5	39.3
CS + SOH	34.2	33.8	36.1	31.6	35.8	31.3	30.9	31.0	28.5
Section B (OH + OCS)	0.0	0.0	0.0	0.0	0.0	0.0	0.0	0.0	0.0
OCSOH (**4**)	1.2	3.2	10.6	8.8	3.3	1.5	3.5	2.8	9.8
OCSOH(**4MP2**)[b]			7.9	7.8	2.6	2.5	4.4	3.5	11.4
TS4MP2/(OH + OCS)[b]			13.2	9.6	6.4	2.8	3.9	2.9	10.7
TS4MP2/(CO + SOH)[b]			13.8	11.1	11.3	8.6	9.6	8.8	16.2
OCSOH (**5**)	−2.2	−1.1	−1.1	−0.6	0.0	0.5	1.6	1.4	7.0
TS5/6	0.8	2.5	10.5	6.3	9.1	4.9	6.6	5.5	13.7
OC(OH)S (**6**)	−30.5	−29.4	−28.7	−27.9	−28.8	−28.0	−26.9	−28.3	−19.5
TS6/7	11.7	12.1	25.0	18.3	21.0	14.3	13.9	12.5	21.4
OC(O)SH (**7**)	−9.0	−7.7	−0.5	−3.7	−0.1	−3.3	−2.0	−3.1	5.1
TS4/(CO + SOH)	7.2	8.8	13.5	10.8	11.2	8.5	10.1	9.3	16.5
OC + SOH	1.3	1.7	−0.1	−2.0	0.5	−1.4	−1.0	−1.0	−3.0
TS7/(CO₂ + SH)	−8.7	−8.0	11.5	2.7	11.2	2.4	3.1	1.7	10.5
CO₂ + SH	−35.8	−35.6	−39.5	−36.5	−37.9	−34.9	−34.7	−34.8	−34.5
Section C(CS₂ + OH + ³O₂)	0.0	0.0	0.0	0.0	0.0	0.0	0.0	0.0	0.0
TS(1 + ³O₂)/8A	**−4.6**	−0.9	35.2	7.7	25.7	−1.8	1.9	0.4	18.5
SC(OO)SOH (**8A**)	−21.2	−16.2	−9.4	−17.5	−20.4	−28.5	−23.5	−25.4	−6.0
TS8A/(OSC + HOSO)	−4.3	0.0	26.6	−1.1	15.4	−12.3	−8.0	−10.3	9.9
OCS + HOSO(**12-cis**)	−110.5	−106.7	−112.4	−107.6	−132.3	−127.5	−123.7	−125.3	−116.8
SC(OO)SOH (**8B**)	−16.5	−11.5	−1.5	−13.8	−9.9	−22.2	−17.2	−19.0	0.1
SC(OO)SOH (**8B′**)	−13.6	−8.9	1.8	−8.5	−8.5	−18.8	−14.1	−16.4	3.6
TS8B/9A	**−7.0**	−5.0	20.3	5.6	7.8	−6.9	−4.9	−7.2	12.6
SCS(OOH)SO (**9A**)	−29.9	−24.0	−16.8	−27.5	−30.4	−41.1	−35.6	−37.5	−18.4
SCS(OOH)SO (**9A′**)	−27.3	−22.0	−14.9	−23.3	−29.5	−37.9	−32.6	−35.0	−14.8
SCS(OOH)SO (**9B**)	−32.0	−26.7	−20.5	−27.9	−36.2	−43.6	−38.3	−40.1	−21.2
TS9A/(OCS + OH + ³SO)[c]	−13.2	−10.2							
TS9B/(OCS + OH + ³SO)[c]	−15.6	−12.9							
OCS + OH + ³SO	−51.9	−51.3	−53.3	−51.7	−60.7	−59.1	−58.5	−58.6	−59.6
SCSO + O₂H	17.9	20.4	28.3	23.3	10.6	5.6	8.1	7.1	14.0
SC(OO)SOH (**8C**)	−11.7	−6.3	7.8	−6.3	−9.1	−23.2	−17.8	−19.7	−0.6
TS8C/10	11.8	15.4	22.3	15.9	9.5	3.1	6.7	4.7	24.1
OSC(O)SOH (**10**)	−81.4	−76.0	−72.0	−77.7	−89.7	−95.4	−90.0	−91.7	−73.1
TS10/(³SO + CO + SOH)	−45.9	−43.3	−41.8	−43.1	−51.8	−53.1	−50.5	−50.8	−38.0
³SO + CO + SOH	−50.6	−49.6	−53.4	−53.6	−60.2	−60.4	−59.4	−59.6	−62.4
TS10/(³SO + OCS + OH)	−51.7	−49.2	−40.7	−43.5	−54.7	−57.5	−55.0	−56.1	−42.3
Section D (³SO + OH)	0.0	0.0	0.0	0.0	0.0	0.0	0.0	0.0	0.0
³SO--OH (**11**)	−3.5	−2.3	13.2	4.2	5.3	−3.7	−2.5	−2.9	3.5
TS11/12	**−2.1**	−1.1	15.1	4.8	8.0	−2.3	−1.3	−2.1	5.5
HOSO (C₁) (**12**)	−58.6	−55.3	−58.8	−55.9	−71.4	−68.5	−65.2	−66.2	−57.8
HOSO (**12-cis**)	−58.6	−55.4	−59.1	−55.9	−71.6	−68.4	−65.2	−66.7	−57.2
HOSO (**12-trans**)	−55.6	−52.4	−53.7	−51.8	−68.8	−66.9	−63.7	−65.2	−55.7
TS12/(SO₂ + H)	−1.8	−3.9	−19.5	−8.7	−27.2	−16.4	−18.5	−19.5	−10.7
TS12/13	**−1.3**	−1.0	6.6	3.0	−10.5	−14.1	−13.8	−15.2	−5.7
HSO₂ (**13**)	−27.6	−24.8	−29.7	−24.0	−49.9	−44.2	−41.4	−42.9	−33.2
TS13/(SO₂ + H)	−3.8	−5.9	−24.8	−13.0	−34.8	−23.0	−25.1	−26.0	−17.7
SO₂ + H	−3.5	−6.1	−29.0	−16.3	−37.7	−25.0	−27.6	−27.8	−25.2
Section E (HOSO + ³O₂)	0.0	0.0	0.0	0.0	0.0	0.0	0.0	0.0	0.0
TS(HOSO + ³O₂/OS(O₂)OH)	2.2	4.2	9.9	3.1	5.6	−1.2	0.8	0.0	11.2
OS(O₂)OH	−1.3	0.8	16.5	0.9	12.0	−3.6	−1.5	−2.1	8.6
TS(OS(O₂)OH/SO₂·O₂H)	0.0	0.2	3.4	1.8	−5.1	−6.7	−6.5	−7.5	3.8
SO₂·O₂H	−5.1	−2.6	−9.4	−9.6	−18.1	−18.3	−15.8	−16.1	−6.5
SO₂ + O₂H	3.3	4.0	−1.8	−2.0	−9.0	−9.2	−8.5	−8.3	−8.7
Section F (CS₂ + ³O₂)	0.0	0.0	0.0	0.0	0.0	0.0	0.0	0.0	0.0
TS(CS₂ + ³O₂)/14	46.1	46.0	118.4	94.9	83.5	60.0	59.9	59.1	67.4
³SC(OO)S (**14**)	38.2	39.2	62.3	42.9	61.4	42.0	43.0	42.2	50.6

[a] Basis set I is 6-31G(d); basis set II is 6-31+G(d); basis set III is 6-311+G(3df,2p). [b] Geometry, zero-point energy, heat capacity correction, and entropy calculated at the MP2/6-31+G(d) level. The zero-point energy is multiplied by 0.95 before computing the zero-point correction. Note that **4** and **4MP2** and **TS4/(CO + SOH)** and **TS4MP2/(CO + SOH)** represent geometries optimized using B3LYP and MP2, respectively. [c] The degree of spin contamination at UHF/6-31G(d) was judged too large to carry out post-SCF calculations.

parameters are compared for a variety of theoretical methods. The key parameter is the S₂–O bond length, where a short bond (~1.75 Å) indicates that the orbitals around sulfur have

rehybridized to allow the formation of a S−OH 2c−2e bond with significant unpaired spin density on sulfur, while a longer S−OH bond (~2.00 Å) would indicate little rehybridization

Atmospheric Oxidation of CS₂

J. Am. Chem. Soc., Vol. 123, No. 10, 2001 2347

Table 2. Geometric Parameters Calculated at Different Levels for the SCSOH Adduct[a]

	B3LYP/II	MP2/I	MP2/II	MP2/III	QCISD(T)/I
S_1C	1.576	1.575	1.573	1.572	1.584
CS_2	1.593	1.612	1.608	1.599	1.617
S_2O	1.797	1.719	1.733	1.727	1.750
OH	0.976	0.979	0.980	0.972	0.980
S_1CS_2	169.2	155.6	157.0	159.8	157.5
CS_2O	111.3	110.4	109.8	111.2	110.2
S_2OH	107.3	106.8	108.3	106.6	106.2
S_1CS_2O	−1.7	−2.1	−1.9	−3.3	−1.6
CS_2OH	80.0	82.6	84.0	77.0	82.5

[a] Basis set I is 6-31G(d), basis set II is 6-31+G(d), and basis set III is 6-311+G(2d,p).

around sulfur with a 2c−3e bond and approximately equal spin density on sulfur and oxygen.[33] The latter type of bond was computed for the Me₂S−OH adduct.[33a] In contrast, for the SCS−OH bond, all methods reveal a much shorter S−OH bond. At the highest level of theory, the QCISD(T)/6-31G(d) optimization (gradients computed by finite-difference energy calculations) gave a S−O bond length of 1.750 Å, somewhat shorter than the B3LYP/6-31+G(d) value (1.797 Å). For all methods, the S_1CS_2O atoms were nearly coplanar with the OH bond rotated about 80° out-of-plane.

The bond enthalpy of SCSOH (S-adduct **1**) is computed to be 6.4 kcal/mol, which is an underestimation by about 3−4 kcal/mol compared to experiment (9.9−10.9 kcal/mol).[5,7] Since rehybrization must precede the 2c−2e OH bond formation, an activation barrier might be expected. However, no barrier could be located at the B3LYP/6-31+G(d) level. To investigate further, a reaction coordinate was computed by varying the S−OH bond and reoptimizing all remaining parameters at the B3LYP/6-31+G(d) level. Single-point energy calculations were made at MP2/6-31+G(d), QCISD(T)/6-31+G(d), and MP2/6-311+G(3df,2p) levels, which were combined to estimate relative energies at the QCISD(T)/6-311+G(3df,2p) level. A plot of the energies (zero-point corrections were not included) in Figure 1 confirms the well-known result that DFT underestimates the activation barrier for many reactions relative to high-level ab initio calculations.[34,35] In the interval of 2.3−2.0 Å, the MP2 method predicts a significant activation barrier (also see Table S2 in Supporting Information). This is the region where rehybrization about sulfur is taking place. The QCISD(T)/6-31+G(d) method reduces the activation due to rehybrization but significantly underestimates the S-adduct bond energy. Combining the ab initio results leads to an activation energy barrier of 0.5 kcal/mol and a bond energy of 7.8 kcal/mol

(33) (a) McKee, M. L. *J. Phys. Chem.* **1993**, *97*, 10971. (b) Braida, B.; Hiberty, P. C.; Savin, A. *J. Phys. Chem. A* **1998**, *102*, 7872. (c) Young, D. C.; McKee, M. L. Bonding in Gas-Phase Sulfur Radicals. In *Computational Chemistry−Reviews of Current Trends*; Leszczynski, J., Ed.; World Scientific: Singapore, 1999. (d) Tureček, F. *Collect. Czech. Chem. Commun.* **2000**, *65*, 455.

(34) (a) In a comparison with experiment of 60 barrier heights, DFT gives barrier heights too low by about 3 kcal/mol. See: Lynch, B.; Fast, P. L.; Harris, M.; Truhlar, D. G. *J. Phys. Chem.* **2000**, *104*, 4811. (b) For a possible explanation for why DFT predicts barrier heights too low, see: Rassolov, V. A.; Ratner, M. A.; Pople, J. A. *J. Chem. Phys.* **2000**, *112*, 4014.

(35) In the analogous reaction H + OCS → OCSH, the DFT barrier is calculated too low by about 4 kcal/mol compared to accurate ab initio. See: Rice, B. M.; Pai, S. V.; Chabalowski, C. F. *J. Phys. Chem. A* **1998**, *102*, 6950.
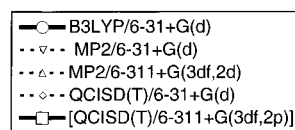

Figure 1. Plot of OH-binding energy (kcal/mol) versus S−OH distance for the OH + CS₂ reaction. The S−OH distance was fixed, and all remaining parameters were optimized at the B3LYP/6-31+G(d) level. Single-point energy calculations were made at the MP2/6-31+G(d), MP2/6-311+G(3df,2d), and QCISD(T)/6-31+G(d) levels. The reaction proceeds without barrier at the B3LYP/6-31+G(d) level. A small barrier of 0.5 kcal/mol is predicted from the composite [QCISD(T)/6-311+G-(3df,2p)] level. Zero-point corrections have not been made.

(without zero-point correction). The composite calculations also predict a weakly bound complex (1.3 kcal/mol) at an S−OH bond distance of about 2.8 Å.

A small positive activation barrier is not consistent with LFP-LIF experiments,[5,7] where a negative enthalpic barrier of 2.3 kcal/mol is determined. There are four possible explanations for this. First, zero-point corrections have not been included; second, the reaction path constructed from DFT optimizations by fixing the S−O bond in SCS−OH at different values may not be appropriate for the [QCISD(T)/6-311+G(3df,2p)] method; third, additional improvement in the level of theory could reduce the energy along the reaction coordinate; and fourth, it is possible that the free energy barrier might be shifted closer to the adduct where the enthalpic contribution is negative (Figure 1).

Returning to the standard computational level, the S-adduct (**1**) is predicted to rearrange to the more stable C-adduct (**2**) with an activation barrier of 15.9 kcal/mol (see Figure 2, **TS1/2**). The C-adduct reacts further to form OCS + SH by first migrating a hydrogen (**TS2/3**) and then cleaving the SH bond (**TS3/(OCS + SH)**). While the OCS + SH products are 34.9 kcal/mol more stable than the OH + CS₂ reactants, the reaction is too slow to be of atmospheric importance due to the initial activation barrier. An alternative pathway **1** → CS + SOH, which cleaves a C−S bond, is endothermic by 37.4 kcal/mol with an activation barrier of 39.9 kcal/mol (**TS1/(CS + SOH)**).

Section B (OH + OCS). The reaction of OH with OCS does not show the O₂ acceleration as found in the OH + CS₂ reaction.[24] The explanation is due to the much smaller stability of the S-adduct **4** (negative bond enthalpy of 2.8 kcal/mol) and the smaller activation barrier to the C-adduct (see Figure 3; 4.1 kcal/mol, **TS5/6**). Wilson and Hirst[36] came to the same conclusion in a G2 study of the OH + OCS reaction. The energetics calculated in their study agree well with the present

(36) Wilson, C.; Hirst, D. M. *J. Chem. Soc., Faraday Trans.* **1995**, *91*, 793.
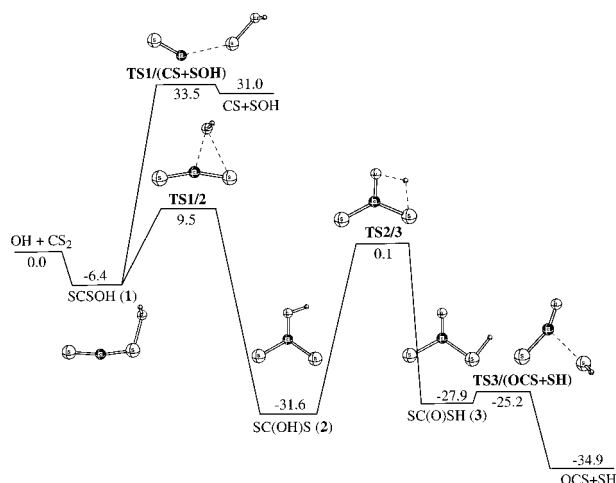
Figure 2. Reaction profile computed at the standard ab initio level (i.e. [QCISD(T)/6-311+G(3df,2p)]//B3LYP/6-31+G(d)+ZPC+heat capacity corrections) for Section A (OH + CS$_2$). Molecular plots are made from the optimized Cartesian coordinates.

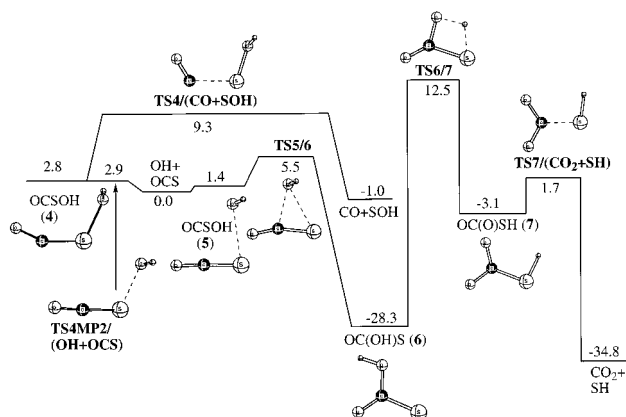**Figure 3.** Reaction profile computed at the standard ab initio level for Section B (OH + OCS).

results (Table 3) except for **TS7/(CO$_2$ + SH)**, which is probably due to the different methods used to compute the transition state geometry (MP2/6-311G(d,p) versus B3LYP/6-31+G(d)).

The S—O distance in the OCSOH S-adduct (**4**) optimized to 1.791 Å at the B3LYP/6-31+G(d) level. However, when **4** was reoptimized using a tighter convergence criterion on the energy gradients, the S—O distance increased substantially (2.644 Å) to give **5**. To further investigate **4**, optimizations were carried out at the MP2/6-31+G(d) level with higher-level single-point calculations and zero-point corrections scaled by 0.95 for **4** (**4MP2**) and the transition states for S—O and S—C bond cleavage (**TS4MP2/OH + OCS** and **TS4MP2/CO + SOH**, respectively). The standard energies of **4** (B3LYP/6-31+G(d) optimized) and **4MP2** (MP2/6-31+G(d) optimized) are within 1.6 kcal/mol of each other, while **TS4/(CO + SOH)** and **TS4MP2/(CO + SOH)** are within 0.3 kcal/mol (Table 1). Using **TS4MP2/(OH + OCS)** to estimate the standard barrier for breaking the S—O bond in **4**, a small value of 0.1 kcal/mol is obtained (Figure 3). The S—OH bond is 2.8 kcal/mol endothermic in **4**, while it is 6.4 kcal/mol exothermic in **1**. Thus, replacing oxygen with sulfur in **1** (giving **4**) has increased the energetic cost of rehybridizing around the sulfur atom such that the strength of the S—OH 2c—2e bond no longer compensates.

The S—OH interaction in **5** is a very weak 2c—3e bond (actually slightly endothermic with respect to OH + OCS) where a total of 0.11β electrons have been transferred from OCS to

Table 3. Comparison of Relative Energies (kcal/mol) at the Standard ab Initio Level and G2 for Species in Section B (OH + OCS) and in Section D (^{3}SO + OH)

	std level[a]	G2(298 K)[b]
Section B (OH + OCS)	0.0	0.0
5	1.4	3.3
TS5/6	5.5	5.0
6	−28.3	−25.7
TS6/7	12.5	12.8
7	−3.1	−0.7
TS7/(CO$_2$ + SH)	1.7	−3.4
CO$_2$ + SH	−34.8	−35.8
TS4/(CO + SOH)	9.3	8.3
CO + SOH	−1.0	−2.4

	std level	G2(0 K)[c,e]	G2(MP2)(298 K)[d,e]
Section D (^{3}SO + OH)	0.0		2.3
SO--OH (**11**)	−2.9		
TS11/12	−2.1		
HOSO (**12**)	−66.2		
TS12/(SO$_2$ + H)	−19.5	−19.5	
TS12/13	−15.2	−16.2	−17.8
HSO$_2$ (**13**)	−42.9	−42.8	−43.3
TS13/(SO$_2$ + H)	−26.0	−29.3/−25.7[f]	−28.0
HOSO (**12-cis**)	−66.7	−66.7	−68.2
HOSO (**12-trans**)	−65.2		−66.4
SO$_2$ + H	−27.8	−27.8	−27.8

[a] [QCISD(T)/6-311+G(3df,2p)]//B3LYP/6-31+G(d)+ZPC and heat capacity corrections to 298 K. [b] Reference 36. [c] Reference 40. [d] Reference 41. [e] All energies are relative to SO$_2$ + H which is assigned a value of −27.8 kcal/mol. [f] Transition state optimized at the QCISD(T) level.

the hydroxyl radical, leaving an excess α electron density on sulfur (B3LYP/6-31+G(d)).

In analogy with the SC(OH)S C-adduct (**2**), OC(OH)S (**6**) can migrate a hydrogen to form OC(O)SH (**7**) and cleave a SH bond to form CO$_2$ + SH. While the reaction **6** → CO$_2$ + SH is exothermic by 6.5 kcal/mol, the step is blocked by a 40.8 kcal/mol barrier. Carbon monoxide can be produced from the reaction of OCS + OH in an exothermic reaction with an activation barrier of 6.5 kcal/mol (**TS4(CO + SOH)**). In a related reaction, it is known that CO is produced from the reaction of S(^{1}D) + OCS.[37]

Section C (CS$_2$ + OH + ^{3}O$_2$). Triplet oxygen is predicted to add readily to SCSOH (**1**) to form the SC(OO)SOH adduct (Figure 4, **8A**).[38] The initial 6.8 kcal/mol activation energy is probably overestimated because the higher-level-correction term (ΔHLC), which corrects for known deficiencies at the QCISD-(T)/6-311+G(3df,2p) level procedure on the basis of the different number of α and β electrons in the reactant and product,[28] has not been included. Thus, it is likely that the SCSOH S-adduct (**1**) has a smaller barrier for addition of ^{3}O$_2$ to form adduct (**8A**) than reaction back to CS$_2$ + OH. This would explain the large enhancement of CS$_2$ loss when OH reacts in the presence of ^{3}O$_2$.

The complex **8** can undergo three different reactions: (1) oxygen atom transfer to the hydroxyl-bearing sulfur; (2) oxygen atom transfer to the unsubstituted sulfur; (3) hydrogen abstraction to form a peroxy group. The first alternative is the lowest-energy pathway (Figure 4, 15.1 kcal/mol), where the transition state closely resembles the suggestion made earlier.[13,14] The O—O breaking bond in the transition state is 1.625 Å, and the forming O—S distance is 1.763 Å, while the C—SOH distance

(37) Richter, R. C.; Rosendahl, A. R.; Hynes, A. J.; Lee, E. P. F. *J. Chem. Phys.* **1998**, *109*, 8876.

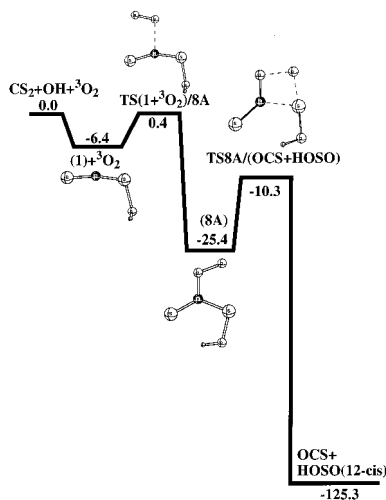(38) A B3LYP/MP2 study of **8A** has recently been reported: Zhang, L.; Qin, Q. *THEOCHEM* **2000**, *531*, 375.

Figure 4. Reaction profile computed at the standard ab initio level for Section C (CS_2 + OH + $^3O_2$) involving the formation of OCS + HOSO via **TS8A/(OCS + HOSO)**.

Figure 5. Reaction profile computed at the standard ab initio level for Section C (CS_2 + OH + $^3O_2$) involving intermediates SC(OOH)-SO (**9**) and OSC(O)SOH (**10**). The energy values for **TS9A(OCS + OH + ^3SO)** (−23.7 kcal/mol) and **TS9B(OCS + OH + ^3SO)** (−26.3 kcal/mol) are determined by adding by the **TS9A(OCS + OH + ^3SO) − 9A** (viz. **TS9B(OCS + OH + ^3SO) − 9B**) energy difference calculated at the B3LYP/6-31+G(d)+ZPC level to the **9A** (viz. **9B**) relative energy computed at the standard level.

has elongated (1.895 Å). In the product direction, the transition vector shows a C−SOH bond lengthening as the oxygen atom is transferred to the sulfur of nascent HOSO fragment. The products, OCS + HOSO, are 125.3 kcal/mol more stable than CS_2 + OH + $^3O_2$ and are the lowest energy species on the potential energy surface.

The SC(OO)SOH complex (**8**) is expected to have multiple conformational minima corresponding to rotations about the O−C, C−S, and O−S bonds. The lowest energy conformer is **8A** in which there is an internal S--HO hydrogen bond. Several stationary points were located on the SC(OO)SOH potential energy surface. The minimum **8B** is important because this conformer is on the reaction path for internal transfer of a hydrogen between two oxygen atoms. Conformer **8B** lacks an internal hydrogen bond presumably because the stabilizing effect of the hydrogen bond does not compensate for the unfavorable cis orientation of the OH bond. A stationary point with an internal O--HO hydrogen bond (**8B′**, C_s-symmetry, not shown) is a transition state 2.6 kcal/mol higher in energy. The transition state for hydrogen transfer (**TS8B/9A**) has C_1 symmetry and is 11.8 kcal/mol higher in energy than **8B**. The transferring hydrogen has distances to oxygen of 1.088 and 1.364 Å. The product, SC(OOH)SO (**9A**), is 12.1 kcal/mol more stable than **8A** and has a nonplanar OH--O hydrogen bond. The planar version of **9A** (**9A′**, C_s-symmetry, not shown) has one imaginary frequency and is 2.5 kcal/mol higher in energy than **9A**. Again, the stabilization of the in-plane hydrogen bond does not compensate for the unfavorable cis orientation of the OH group. The O−H bond is 1.751 Å in **9A′** and 1.979 Å in **9A**. The lowest energy SC(OOH)SO isomer is **9B** which is 2.6 kcal/mol lower than **9A**.

Transition states for fragmentation of **9A,B** were calculated via **TS9A/(OCS + OH + ^3SO)** and **TS9B/(OCS + OH + ^3SO)**, respectively. Both transition states have a high amount of spin contamination which is understandable due to the products which have doublet and triplet spin states (OH and ^3SO). In **TS9A/(OCS + OH + ^3SO)** ($<S^2>$ = 1.40, B3LYP/6-31+G(d)), the forming OH and ^3SO fragments have 0.74β and 0.90α unpaired spin electrons, respectively, while the corresponding values in **TS9B/(OCS + OH + ^3SO)** ($<S^2>$ = 1.16, B3LYP/6-31+G(d)) are 0.55β and 1.35α unpaired spin electrons, respectively. The breaking O−O and C−S bonds are rather unequal in **TS9A/(OCS + OH + ^3SO)** (1.953 and 1.822 Å) which is in contrast to the O−O and C−S bonds in **TS9B/**
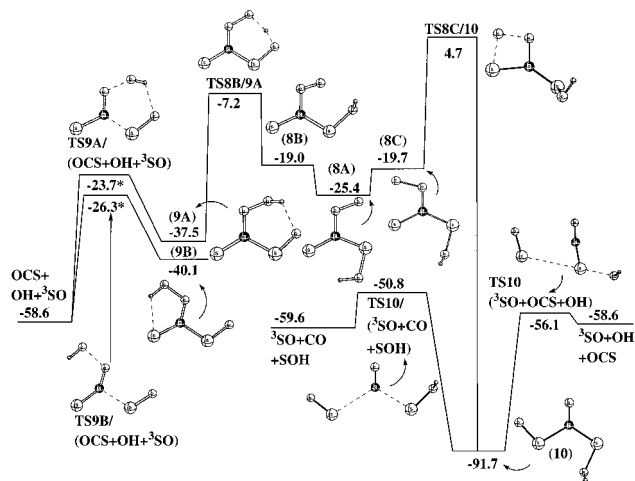
(OCS + OH + ^3SO) where they are broken to approximately the same extent (1.808 and 2.098 Å).

The spin contamination of **TS9A/(OCS + OH + ^3SO)** and **TS9B/(OCS + OH + ^3SO)** was deemed too large to carry out the MP2 and QCISD(d)/6-31G(d) ab initio calculations. To estimate the relative energies of the two transition states, the computed fragmentation barriers for **9A** (13.8 kcal/mol) and **9B** (13.8 kcal/mol) calculated at the B3LYP/6-31+G(d)+ZPC level (Table 1) were added to the standard relative energy of **9A** (−37.5 kcal/mol, Figure 5) and **9B** (−40.1 kcal/mol, Figure 5) to give the estimated relative energy of **TS9A/(OCS + OH + ^3SO)** (−23.7 kcal/mol) and **TS9B/(OCS + OH + ^3SO)** (−26.3 kcal/mol).

The reaction SC(OOH)SO (**9B**) → SCSO + O₂H is not expected to be a potential source of O₂H radical. The C−OOH bond enthalpy (298K) in **9B** is calculated to be 47.2 kcal/mol (Table 1).

An alternative decomposition pathway from **8** was explored (Figure 5). The first step is formation of the less stable conformer of SC(OO)SOH (**8C**), which is 5.7 kcal/mol higher in energy than **8A**. From this conformer, an oxygen atom can be transferred in **TS8C/10** to form OSC(O)SOH (**10**) (Figure 5), where the driving force of the reaction is the formation of a C=O double bond.

Two transition states were located for decomposition of **10**, **TS10/(^3SO + OCS + OH)** and **TS10/(^3SO + CO + SOH)**, both of which were also characterized with significant spin contamination ($<S^2>$ = 1.65 and 1.61, respectively, B3LYP/6-31+G(d)). In the former case, the transition state **TS10/(^3SO + OCS + OH)** is 2.5 kcal/mol less stable than fragments, while, in the latter case, the transition state **TS10/(^3SO + CO + SOH)** is 8.8 kcal/mol above fragments. The corresponding values at the B3LYP/6-31+G(d)+ZPC level are very similar, 2.0 and 6.3 kcal/mol, respectively. Although not investigated in the present study, the thermodynamic stability of **10** may be sufficient to allow bimolecular reaction with molecular oxygen to form such products as SO₂ + OCS + O₂H which might contribute to the "prompt" formation of SO₂. The alternative/additional source of "prompt" SO₂ would be from

Figure 6. Reaction profile computed at the standard ab initio level for Section D (^{3}SO + OH).

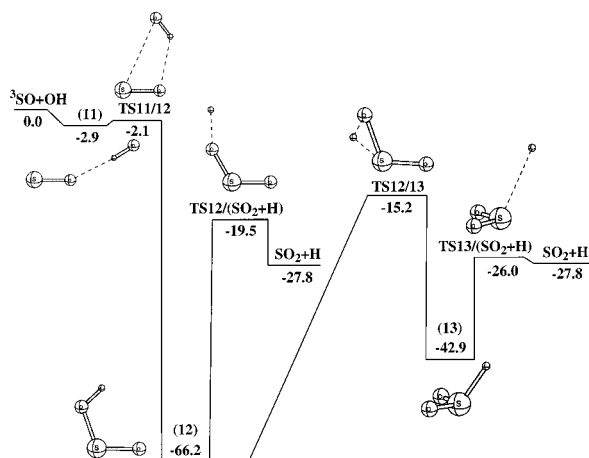**Figure 7.** Reaction profile computed at the standard ab initio level for Section E (HOSO + ^{3}O$_2$).

direct formation of HOSO (via **TS8A/(OCS + HOSO)**) which would give SO$_2$ after hydrogen abstraction with molecular oxygen.

Section D (^{3}SO + OH). While it is not an important reaction in the atmosphere, the reaction of ^{3}SO with OH radical (Figure 6) may have contributed to formation of SO$_2$ in the laboratory study of Stickel et al.[14] The initial reaction is formation of a hydrogen-bonded complex (**11**) 2.9 kcal/mol more stable than OH + ^{3}SO.[39] Like the reactant and transition state in the SCSOH + ^{3}O$_2$ reaction, the reactant and initial complex have a different number of α and β electrons. Thus, the G2(MP2,-SVP) method would stabilize the complex by an additional 3.1 kcal/mol relative to OH + ^{3}SO, making the hydrogen bond in **11** stronger than 3 kcal/mol. The transition state (**TS11/12**) for formation of HOSO (**12**) is only 0.8 kcal/mol with respect to the complex.

The initial stage of reaction is comprised of rather complicated coupling of electrons. For that reason, the reaction was also studied with MCSCF and will be discussed separately below. The MCSCF results are in good quantitative agreement with the standard ab initio values.

The HOSO (**12**) radical can lose a hydrogen with a barrier of 46.7 kcal/mol. The reverse reaction, addition of H to one oxygen of SO$_2$, has a barrier of 8.3 kcal/mol. The transition state for migration of hydrogen between the oxygen and sulfur atoms of SO$_2$ was located 51.0 kcal/mol higher in energy than HOSO (**12**). The product HSO$_2$ (**13**) is 23.3 kcal/mol less stable than **12**. Elimination of hydrogen from HSO$_2$ (**13**) to form SO$_2$ + H is predicted to have a forward barrier of 16.9 kcal/mol and a reverse barrier of 1.8 kcal/mol. Thus, the lowest energy pathway **12** → **13** is to eliminate hydrogen from **12** (**TS12/(SO^2 + H)**) and then add hydrogen to SO$_2$ (**TS13/(SO$_2$ + H)**). Very similar results were obtained by Marshall and co-workers[40] at the G2 level for various parts of the SO$_2$ + H potential energy surface (Table 3). The major difference between G2 and the present results is the level of theory used for geometry optimization, MP2/6-31G(d) and B3LYP/6-31+G-(d), respectively. At the B3LYP/6-31+G(d) level, HOSO is predicted to have C_1 symmetry; the cis and trans structures are

both transition states, while, at the MP2/6-31G(d) level, the HOSO cis structure is the only H−O−S−O minimum. Also, at the G2 level the **TS13/(SO$_2$ + H)** transition state is predicted to be more stable than SO$_2$ + H (−1.5 kcal/mol, Table 3), which is in contrast to the current results. However, when the **TS13/(SO$_2$ + H)** G2-energy is evaluated at the QCISD(T) geometry rather than the MP2 geometry (2.1 kcal/mol), better agreement is found with the present results. Frank et al.[41] studied the decomposition of HOSO (**11**) using neutralization−reionization mass spectrometry. They found that the main products were OH and SO rather than the more thermodynamically stable products SO$_2$ + H.

Section E (HOSO + ^{3}O$_2$). The HOSO isomer (**12**) can react with ^{3}O$_2$ to form SO$_2$ plus O$_2$H in a reaction that is 8.3 kcal/mol exothermic (Figure 7). There are strong parallels between this reaction and the hydrogen abstraction reaction in eq 5, where the latter reaction has been studied extensively due to its importance in hydrocarbon combustion.[42] At the CCSD(T)/TZ2P//CCSD(T)/DZP + ZPC level,[42] the barrier to form the ethylperoxy radical (CH$_3$CH$_2$OO) is 0.2 kcal/mol, while the enthalpy of the second transition state to eliminate O$_2$H is only 0.2 kcal/mol higher than C$_2$H$_5$ + ^{3}O$_2$ and the overall reaction is exothermic by 13.0 kcal/mol. The HOSO + ^{3}O$_2$ reaction has an initial barrier of 0.0 kcal/mol at the standard level to form a weakly bound OS(O$_2$)OH complex (−2.1 kcal/mol, Figure 7). It is interesting that the S−O distance in the addition complex (1.995 Å) is actually longer than the S−O distance in the OS-(O$_2$)OH complex (2.122 Å). The stabilizing feature in the OS-(O$_2$)OH complex is the formation of a O--H hydrogen bond (1.648 Å). The small barrier for hydrogen atom transfer at the B3LYP/6-31+G(d) level (1.3 kcal/mol, Table 1) completely disappears at the standard level of theory. The product is a SO$_2$·O$_2$H complex, bound by a hydrogen bond 7.8 kcal/mol more stable than SO$_2$ + O$_2$H and a O--H distance of 1.734 Å. Thus, the calculations unambiguously predict that HOSO will form SO$_2$ rapidly and almost quantatively in the presence of ^{3}O$_2$.

$$C_2H_5 + {}^3O_2 \rightarrow CH_3CH_2OO \rightarrow C_2H_4 + O_2H \qquad (5)$$

(39) (a) It is interesting to point out the analogy between ^{3}SO + OH → HOSO and the reaction ^{3}O$_2$ + OH → HOOO.[37b−d] (b) Speranza, M. *J. Phys. Chem. A* **1998**, *102*, 7535. (c) Aloisio, S.; Francisco, J. S. *J. Am. Chem. Soc.* **1999**, *121*, 8592. (d) Garrido, J. D.; Caridade, P. J. S. B.; Varandas, A. J. C. *J. Phys. Chem. A* **1999**, *103*, 4815. (e) Nelander, B.; Engdahl, A.; Svensson, T. *Chem. Phys. Lett.* **2000**, *332*, 403.
(40) Goumri, A.; Rocha, J. D. R.; Laakso, D.; Smith, C. E.; Marshall, P. *J. Phys. Chem. A* **1999**, *103*, 11328.
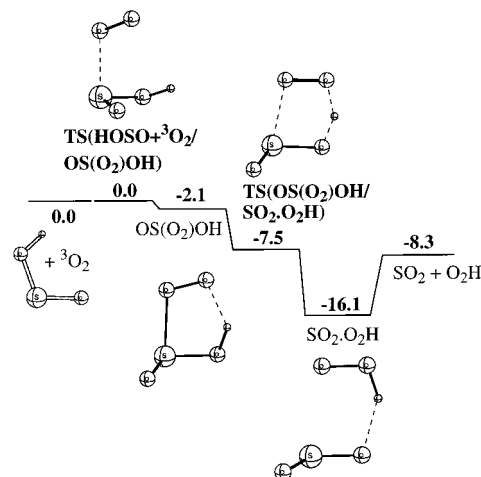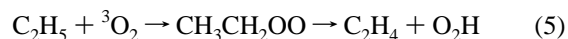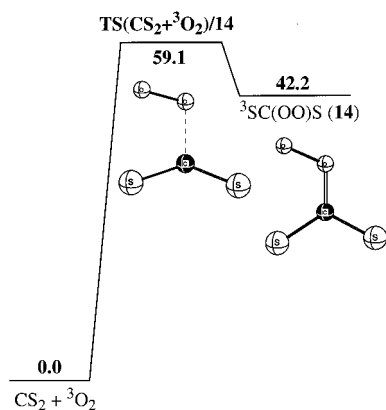
(41) (a) Frank, A. J.; Sadílek, S.; Ferrier, J. G.; Tureček, F. *J. Am. Chem. Soc.* **1996**, *118*, 11321. (b) Frank, A. J.; Sadílek, S.; Ferrier, J. G.; Tureček, F. *J. Am. Chem. Soc.* **1997**, *119*, 12343.
(42) (a) Rienstra-Kiracofe, Allen, W. D.; Schaefer, H. F. *J. Phys. Chem. A* **2000**, *104*, 9823 and extensive citations therein. (b) Also see: Clifford, E. P.; Farrell, J. T.; DeSain, J. D.; Taatjes, C. A. *J. Phys. Chem. A* **2000**, *104*, 11549.

Table 4. Important Configurations in the Wave Function for the ^{3}SO + OH Complex (**11**) and Transition State **TS11/12** at the CAS(11e,7o)/6-31+G(d) Level
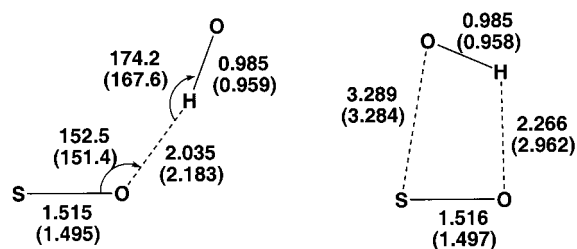
^{3}SO/OH complex (**11**)				^{3}SO+OH transition state (**TS11/12**)		
config	weight[a]	model[b]	frag. descript.	config	weight[a]	model[b]
1,2	70.7		SO + OH	1	41.1	
3	12.8		SO$^+$ + OH$^-$	2	30.2	
4	11.9		SO$^-$ + OH$^+$	3,4	24.1	
5	4.1		SO$^+$ + OH$^-$			

[a] Percent contribution of configuration to wave function. [b] Each p lobe corresponds to an orbital except for the σ_{SO} and σ^*_{SO}, where the two p lobes form bonding and antibonding combinations. In the CAS(11e,7o)/6-31+G(d) calculation, there are 11 electrons to distribute into 7 orbitals. The electrons couple into an overall ^{2}A″ state.

Figure 8. Reaction profile computed at the standand ab initio level for Section F (CS$_2$ + ^{3}O$_2$).

Figure 9. Comparison of calculated geometric parameters for the ^{3}SO + OH complex (**11**) and the transition state **TS11/12** by B3LYP/6-31+G(d) and CAS(11e,7o)/6-31+G(d) (in parentheses) levels of theory.

Section F (CS$_2$ + ^{3}O$_2$). The reaction of CS$_2$ with ^{3}O$_2$ (Figure 8) has a large activation barrier (59.1 kcal/mol) and endothermicity (42.2 kcal/mol). The transition state (**TS(CS$_2$ + ^{3}O$_2$/ 14)**) is a triplet with little spin contamination ($<S^2>$ = 2.02, B3LYP/6-31+G(d)) which means the calculated barrier should be reliable. The high activation barrier emphasizes the importance of the SCSOH (**1**) adduct in the overall reaction mechanism. Even though the OH binding is small, the adduct causes a shift of unpaired electron density toward the carbon atom which causes a reduction in the barrier for ^{3}O$_2$ addition from 59.1 kcal/mol to 6.8 kcal/mol.

MCSCF Calculations ^{3}SO + OH and SCSOH (1) + ^{3}O$_2$. MCSCF calculations were carried out for two steps, OH + ^{3}SO and SCSOH (**1**) + ^{3}O$_2$. At the B3LYP/6-31+G(d) level, the initial ^{3}SO + OH complex (**11**) and transition state (**TS11/12**) had spin-squared values of $<S^2>$ = 1.76 and $<S^2>$ = 1.75 (B3LYP/6-31+G(d)), respectively, rather than the expected value of $<S^2>$ = 0.75 which indicates significant spin contamination. Thus, in analogy with a UDFT treatment of a singlet biradical where the $<S^2>$ value approaches 1.00, the

current UDFT treatment of a doublet (with two loosely coupled electrons) approaches an $<S^2>$ value of 1.75 (0.75 + 1.00).

Since the expected spin-squared values were not obtained, geometries and frequencies were determined at the complete active space CAS(11e,7o)/6-31+G(d) level. Both methods are in good agreement with the structure of the complex and transition state. The H--O hydrogen-bonded distance in the complex (**11**) is slightly longer (Figure 9) at the CAS level (2.183 Å) compared to DFT (2.035 Å). In the transition state (**TS11/12**), the forming S--O distance is nearly the same by both methods (3.28 Å) while the H--O hydrogen-bonded distance shows less similarity (2.962 Å, CAS; 2.266 Å, DFT).

The CAS calculations used 6 electrons in 4 orbitals for ^{3}SO and 5 electrons in 3 orbitals for the hydroxyl radical. For the complex and transition state, the distribution of electrons within the seven orbitals is depicted in Table 4. Each molecular orbital is shown as a single in-plane or out-of-plane p orbital. The occupation is indicated by the number of dots within the orbital. In the transition state, the solid line indicates a bonding orbital, while the dashed line indicates a single antibonding orbital between the sulfur and oxygen atoms. In the complex, two configurations, constituting 70.7% of the wave function, are characterized by three singly occupied orbitals and corresponds to the interaction of two neutral species. Configurations 3–5

Table 5. Relative Energies (kcal/mol) at CAS(11e,7o)/6-31+G(d) for the Addition of OH to ^{3}SO and at CAS(3,3)6-31+G(d) for the Addition of $^3O_2$ to SCSOH

	CAS(e,o)	CAS(6-31+G(d))	+ZPE	ΔH(298 K)	$[\Delta H$(298 K)$]^a$
^{3}SO + OH	(11,7)	0.0	0.0	0.0	0.0
complex **11**	(11,7)	−2.6	−1.6	−1.9	−2.9
TS11/12	(11,7)	−0.4	−0.4	−0.9	−2.1
SCSOH + $^3O_2$	(3,3)	0.0	0.0	0.0	0.0
TS(SCSOH + $^3O_2$/8A)	(3,3)	3.8	3.8	3.4	2.2

^{a} Standard ab initio level (Table 1).

correspond to charge-transfer configurations where an electron has been transferred between fragments to allow increased donor−acceptor interaction. In configurations 3 and 4, constituting 24.7% of the wave function, two additional electrons have coupled to occupy one molecular orbital.

In the transition state, the oxygen end of the hydroxyl radical swings around so that the radical center can interact with an in-plane p-orbital on sulfur. Configurations 1 (41.1%) and 2 (30.2%) correspond to the bonding and antibonding combination, respectively, of the two interacting p orbitals. The contribution of the two configurations is similar due to the large distance between the two centers (3.28 Å). For the transition state, 24.1% of the wave function is composed of configurations with three open shells. It is satisfying that the CAS and ab initio results agree with the complexation energy and barrier height to about 1 kcal/mol (Table 5).

The DFT calculations on the transition state (**TS(1 + $^3O_2$)/8A**) for addition of $^3O_2$ to SCSOH (**1**) also suffered from spin contamination ($<S^2> = 0.91$, B3LYP/6-31+G(d)) but not to the same extent as **TS11/12**. A 2-electrons in 2-orbitals active space was used for molecular oxygen, and a ROHF calculation was used for the SCSOH (**1**) radical. The transition state was located with a CAS(3e,3o) and confirmed by calculating vibrational frequencies. Two configurations, comprising 93% of the wave function, were characterized by one open-shell which indicates significant coupling of electrons in the transition state. The forming C--O bond is predicted to be 2.335 Å by CAS and 2.105 Å by DFT. One of the two dominant configurations (73% contribution) has the σ_{CO} molecular orbital doubly occupied, while the other (20% configuration) has the σ^*_{CO} molecular orbital doubly occupied. Again, the CAS and standard ab initio levels agree with the predicted barrier height to about 1 kcal/mol (Table 5).
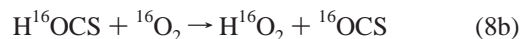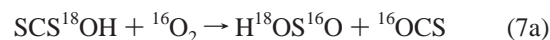
Implication for Interpretation of Key Laboratory Experiments. It is instructive to consider the present computational results in the light of recent experiments. Lovejoy et al.,[9] using a pulsed photolysis technique, have measured the yield of O_2H in the CS_2/OH/O_2 reaction to be 95 ± 15% of the OH consumed. In addition, using chemical ionization mass spectrometric (CIMS) detection, they determined that the production of O_2H and SO_2 was directly correlated. The reaction HOSO + $^3O_2$ → SO_2 + O_2H (eq 3d) was not considered because earlier ab initio work[43] predicted the reaction to be endothermic by 26 kcal/mol.

The large energy release associated with conversion of SCSOH + $^3O_2$ to HOSO + OCS (Figure 4) suggests that the products are likely to be produced with significant internal excitation. The small yield of prompt CO observed by Stickel et al.[14] could result from fast decomposition of a small fraction of OCS that is formed with sufficiently large vibrational excitation (74 kcal/mol is required). The sulfur atom produced via OCS dissociation reacts rapidly with $^3O_2$ to produce ^{3}SO

which, in turn, reacts slowly with $^3O_2$ to produce SO_2, thus potentially accounting for about half of the nonprompt SO_2 observed by Stickel et al.[14] A potential source of the remaining nonprompt SO_2 is ^{3}SO which could be generated from decomposition of a small fraction of HOSO that is formed with sufficiently high vibrational excitation. Clearly, future experimental and theoretical studies of energy partitioning in the products of the SCSOH + $^3O_2$ reaction are needed to test the possibilities suggested above.

Another revealing experiment by Lovejoy et al.[6] used OD rather than OH in the CS_2/OD/O_2 reaction to determine the deuterium isotope effect. The LFP-LIF experiments showed that the kinetic isotope effect was 1 within experimental error ($k_H/k_D = 1.05 ± 0.18$) which indicates that a hydrogen bond forming or breaking reaction cannot be part of the rate-determining step. In the mechanism presented in eqs 3a−e, the lowest-energy process is the reaction from **8A** to OCS + HOSO with a barrier of only 15.1 kcal/mol. In comparison, the hydrogen migration step to form SC(OOH)SO (**9A**) is uphill by 18.2 kcal/mol with respect to **8A**.

In a labeling study, Lovejoy et al.[13] used ^{18}OH instead of ^{16}OH in the CS_2/^{18}OH/O_2 reaction and found that $^{16}OS^{18}O$ is the dominant SO_2 isotopomer. They presented three alternative sequences of reactions which could explain the observed products:

$$SCS^{18}OH + {}^{16}O_2 \rightarrow H^{16}O_2 + CS_2{}^{18}O \qquad (6a)$$

$$CS_2{}^{18}O + {}^{16}O_2 \rightarrow {}^{16}OCS + {}^{16}OS^{18}O \qquad (6b)$$

$$SCS^{18}OH + {}^{16}O_2 \rightarrow H^{18}OS^{16}O + {}^{16}OCS \qquad (7a)$$

$$H^{18}OS^{16}O + {}^{16}O_2 \rightarrow H^{16}O_2 + {}^{16}OS^{18}O \qquad (7b)$$

$$SCS^{18}OH + {}^{16}O_2 \rightarrow H^{16}OCS + {}^{16}OS^{18}O \qquad (8a)$$

$$H^{16}OCS + {}^{16}O_2 \rightarrow H^{16}O_2 + {}^{16}OCS \qquad (8b)$$

The currently proposed mechanism (eqs 3a−e) is consistent with eqs 7a,b.

The overall reaction, OH + 2^3O_2 + CS_2 → OCS + SO_2 + O_2H, has an experimental[44] exothermicity of −138.8 kcal/mol which can be compared to a calculated value (at the standard level) of −139.5 kcal/mol.

Conclusions

Density functional theory, in conjunction with conventional ab initio theory, has been used to study reactions relevant to the atmospheric oxidation of CS_2. The computational method

(43) Boyd, R. J.; Gupta, A.; Langler, R. F.; Lownie, S. P.; Pincock, J. A. *Can. J. Chem.* **1980**, *58*, 331.

(44) DeMore, W. B.; Sander, S. P.; Howard, C. J.; Ravishankara, A. R.; Golden, D. M.; Kolb, C. E.; Hampson, R. F.; Kurylo, M. J.; Molina, M. J. *Chemical Kinetics and Photochemical Data for Use in Stratospheric Modeling*; JPL: Pasadena, CA, 1997; JPL 97-4, No. 12.

is of similar quality as the G2(MP2,SVP) procedure which is normally quite reliable for ground-state energetics. However, several of the transition states suffered from spin contamination which could increase uncertainties in their barrier heights. The largest deviation from the expected spin-squared value was encountered in the ^{3}SO + OH reaction. When this reaction was also studied by a multiconfigurational method (CAS(11e,7o)/6-31+G(d)), results very similar to methods based on a single reference were obtained.

The addition of OH to CS₂ to form the S-adduct (**1**) is predicted to occur without activation at the density functional level but with a small activation barrier when more accurate methods are applied. It appears that DFT underestimates the energy costs of electron reorganization in the early stage of bond formation.

The reaction of the SCS−OH adduct (**1**) with O₂ is shown to proceed efficiently via addition of O₂ to the carbon atom (to form **8A**); this reaction is probably the rate-determining step in conversion of **1** to observed end products. An energetically favorable path has been found for the conversion of SCSOH + ^{3}O₂ to HOSO + OCS. The prompt products O₂H and SO₂ observed in laboratory studies[9,14] can be generated from HOSO + ^{3}O₂ reaction, which is an exothermic, barrierless process. The prompt product CO observed in laboratory studies[9] *could* be generated via decomposition of a small fraction of OCS that is generated with significant internal excitation, a possibility that remains to be tested through future experimental and theoretical research.

Supporting Information Available: Absolute energies (hartrees) and zero-point energies (kcal/mol) at B3LYP/6-31+G(d) optimized geometries (Table S1), relative energies (kcal/mol) at B3LYP/6-31+G(d), MP2/6-31+G(d), MP2/6-311+G(3df,2p), QCISD(T)/6-31+G(d), and [QCISD(T)/6-311+G(3df,2p)] levels for SCSOH along the S−OH reaction reaction coordinate (Table S2), absolute energies (hartrees) and zero-point energies at the CAS(11e,7o)/6-31+G(d) level for the addition of OH to ^{3}SO and at the CAS(3,3)/6-31+G(d) level for the addition of ^{3}O₂ to SCSOH (Table S3), and Cartesian coordinates for relevant structures optimized at the B3LYP/6-31+G(d) level (Table S4) (PDF). This material is available free of charge via the Internet at http://pubs.cas.org.